Dynamic temperature modeling of an SOFC using least squares support vector machines

Ying-Wei Kang [a,*], Jun Li [a], Guang-Yi Cao [a],
Heng-Yong Tu [a], Jian Li [b], Jie Yang [b]

[a] *Institute of Fuel Cell, Shanghai Jiao Tong University, Shanghai 200240, China*
[b] *School of Materials Science and Engineering, Huazhong University of Science and Technology, Wuhan 430074, China*

Abstract

Cell temperature control plays a crucial role in SOFC operation. In order to design effective temperature control strategies by model-based control methods, a dynamic temperature model of an SOFC is presented in this paper using least squares support vector machines (LS-SVMs). The nonlinear temperature dynamics of the SOFC is represented by a nonlinear autoregressive with exogenous inputs (NARXs) model that is implemented using an LS-SVM regression model. Issues concerning the development of the LS-SVM temperature model are discussed in detail, including variable selection, training set construction and tuning of the LS-SVM parameters (usually referred to as hyperparameters). Comprehensive validation tests demonstrate that the developed LS-SVM model is sufficiently accurate to be used independently from the SOFC process, emulating its temperature response from the only process input information over a relatively wide operating range. The powerful ability of the LS-SVM temperature model benefits from the approaches of constructing the training set and tuning hyperparameters automatically by the genetic algorithm (GA), besides the modeling method itself. The proposed LS-SVM temperature model can be conveniently employed to design temperature control strategies of the SOFC.
© 2008 Elsevier B.V. All rights reserved.

Keywords: Solid oxide fuel cell (SOFC); Dynamic temperature model; Least squares support vector machine (LS-SVM); Hyperparameter tuning; Genetic algorithm (GA)

1. Introduction

The solid oxide fuel cell (SOFC) is expected to be one of the most promising devices for energy conversion because of its high efficiency, low pollutant emissions and flexible fueling strategies. Possible applications of SOFCs range from vehicular auxiliary power units to stationary power plants [1]. Cell temperature control plays a crucial role in SOFC operation [2,3]. This is because the cell temperature has a significant effect on the electrical characteristics of an SOFC, e.g. the cell voltage and the current density distribution. Moreover, the variation of cell temperature may cause degradation, even damage to the fuel cell due to thermal fatigue or thermal cracking of the cell material. Thus, the average cell temperature should be carefully controlled. In order to design effective temperature control strategies by using model-based control methods, simple and accurate dynamic temperature models of SOFCs are highly desired.

In recent years, many dynamic physical models of SOFCs based on conservation laws and electrochemical principles have been reported [3–6]. Although these models are useful for the analysis and optimization of SOFCs, in general they are too complex for applying model-based control methods. The complicated phenomena associated with SOFCs easily drive such models to high complexity [7]. Developing simpler data-driven models based on the system identification methodology is an important way to control complex plants [8,9]. Following this line, many data-driven modeling approaches, such as classical system identification, artificial neural networks (ANNs) and fuzzy logic, can be applied to dynamic temperature modeling of SOFCs. The requirements for developing such data-driven temperature models of SOFCs for control purpose can be summarized as:

---

* Corresponding author. Tel.: +86 21 34206249; fax: +86 21 34206249.
E-mail address: yingwei.kang@gmail.com (Y.-W. Kang).

Nomenclature

A	cell active area (m^2)
A_r	reforming reaction surface area (m^2)
A_{sh}	anode section area (m^2)
AR	air ratio
b	bias term
$b_0–b_3$	fitting function coefficients of specific heat capacity
c_p	specific heat capacity of gas species ($J\,mol^{-1}\,K^{-1}$)
C_p^s	specific heat capacity of solid part ($J\,kg^{-1}\,K^{-1}$)
e_k	prediction error of the kth data point
E_a	activation energy ($J\,mol^{-1}$)
F	Faraday's constant (=96,485 $C\,mol^{-1}$)
h_i	molar enthalpy ($J\,mol^{-1}$)
ΔH	total change of molar enthalpy for chemical reaction ($J\,mol^{-1}$)
J	average current density ($A\,m^{-2}$)
k_p	coefficient for unit conversion (=10^5 $Pa\,bar^{-1}$)
k_r	reforming reaction constant (=4274 $mol\,s^{-1}\,m^{-2}\,bar^{-1}$)
k_{sh}	WGS reaction constant (=1.2×10^4 $mol\,m^{-3}\,s^{-1}$)
K	kernel function
K_{sh}	equilibrium constant of WGS reaction
M^s	mass of solid part (kg)
n_e	number of transferred electrons
n_i	molar number of species i within SOFC (mol)
n_y, n_d, n_u	maximum lags
N	molar flow rate ($mol\,s^{-1}$), number of data points
p	pressure (bar)
P_{dc}	direct current electric power (W)
r_j	rate of reaction j ($mol\,s^{-1}$)
R	universal gas constant (=8.314 $J\,mol^{-1}\,K^{-1}$)
R_{ohm}	total cell resistance ($\Omega\,m^2$)
T	temperature (K)
T_0	initial temperature (K)
U	voltage (V)
U_f	fuel utilization
V	volume (m^3)
$\boldsymbol{w}$	feature vector
$\boldsymbol{x}$	input vector
x_i	molar fraction of species i
y	output value

Greek symbols

α_k	Lagrange multiplier
β_{an}, β_{ca}	pre-exponential factors of anode and cathode ($A\,m^{-2}$)
η	overpotential (V)
$\boldsymbol{\varphi}$	nonlinear mapping
γ	regularization parameter
σ	kernel parameter
$\sigma_{an}, \sigma_{ca}, \sigma_{elec}$	electrical conductivity of anode, cathode and electrolyte ($\Omega^{-1}\,m^{-1}$)
τ	thickness (m)

ξ	number of chemical reactions
ζ	number of gases

Subscripts

act	activation
an	anode
ca	cathode
conc	concentration
elec	electrolyte
i	gas species i
j	the jth reaction
k	sampling instant k, the kth data point
ohm	ohmic
r	steam reforming reaction
sh	water–gas shift reaction

Superscripts

in	fuel cell inlet
out	fuel cell outlet
ref	reference condition
s	solid part (including the PEN and interconnect)

(1) The model should be able to represent the temperature dynamics of an SOFC accurately over a relatively wide operating range, certainly including the design point.

(2) The model can be conveniently integrated into the whole control scheme of an SOFC.

(3) The model's performance should be fully tested over the expected operating range.

(4) The modeling process should be as simple as possible.

Compared with the substantial progress on physical modeling, however, data-driven dynamic temperature models of fuel cells (particularly of SOFCs), which meet all above requirements, are still rare.

Shen et al. [10] presented an application of radial basis functions (RBFs) neural networks to develop a dynamic temperature model of a molten carbonate fuel cell (MCFC) stack. Although satisfactory degree of precision is obtained, the MCFC RBF-NN model has several weaknesses. First, the topology and training strategy of RBF-NNs are determined by experience, which weakens the model's objectivity. Second, RBF-NNs get easily stuck in local extrema. Third, the effect of load disturbance on cell temperature was left out of consideration, which impairs the model's generality. Jurado [11,12] used different Hammerstein models to represent the dynamic characteristics of an SOFC. As the Hammerstein model, which uses a static nonlinear block followed by a dynamic linear block to represent nonlinear systems, is a special type of nonlinear model, these SOFC models still need more tests over a wide operating range. Yang et al. [13] reported a dynamic T–S fuzzy model of a MCFC, which consists of a voltage and a temperature submodel. However, the temperature submodel can only be valid within a relatively narrow temperature range. In addition, the identification procedure

of the T–S model, which contains an antecedent identification and a consequent identification, is complicated.

As an important breakthrough in the area of machine learning in the last decade, the support vector machine (SVM) has proven to be a powerful tool for solving classification and regression problems. However, the training of SVM needs to solve a quadratic programming (QP) problem, which is time-consuming in the case of large data set. The least squares support vector machine (LS-SVM), which achieves the solution by solving a set of linear equations, is a least squares version of standard SVM [14]. Compared with SVM, it can significantly reduce the training time at the price of just a small precision loss [14]. Moreover, it maintains SVM's advantages of superior generalization ability and finding global solution. In recent years, the LS-SVM method has aroused interests of many researchers [15–17], and has already been used to model the static voltage characteristics of an SOFC [18].

In this paper, a dynamic temperature model of an SOFC, which aims to satisfy all the above modeling requirements, is built using the LS-SVM regression method. The nonlinear temperature dynamics of the SOFC is represented by a nonlinear autoregressive with exogenous inputs (NARXs) model [9] that is implemented using an LS-SVM regression model. In this study, the training data is generated with a physical model of an SOFC. A training set covering the entire expected operating range is constructed. To improve the resulting model's generalization ability, an innovative optimization algorithm known as the genetic algorithm (GA) [19,20] are adopted to automatically tune two parameters in LS-SVM design (usually referred to as hyperparameters). In addition, the LS-SVM temperature model is fully tested over the operating range by comparison with the physical model.

The rest of this paper is organized as follows. In Section 2, the SOFC process is briefly described. In Section 3, the development of the dynamic temperature model using LS-SVMs is presented in detail. Modeling results and model validation are presented in Section 4. Finally, conclusions are drawn in Section 5.

2. Description of SOFC process

The SOFC can be viewed as a electrochemical reactor operating at very high temperatures (600–1000 °C), which produces electricity and heat directly from the electrochemical combination of a gaseous fuel (hydrogen or hydrocarbons, e.g. methane) with an oxidant (typically air). An SOFC consists of an interconnect structure and a tri-layer structure composed of two porous ceramic electrodes, anode and cathode, separated by a dense ceramic electrolyte (often referred to as the PEN). The operating principle of an SOFC process may be described in Fig. 1. Fuel and air are fed into the anode and cathode channels, respectively. At the cathode, oxygen is consumed to form oxygen ions by obtaining electrons. The oxygen ions migrate through the ion-conducting electrolyte to the anode where they combine with hydrogen, producing water vapor and releasing electrons to the external circuit. The released electrons are transferred to the cathode via an external load, where they perform electrical work. The electrochemical reactions for the anode and cathode
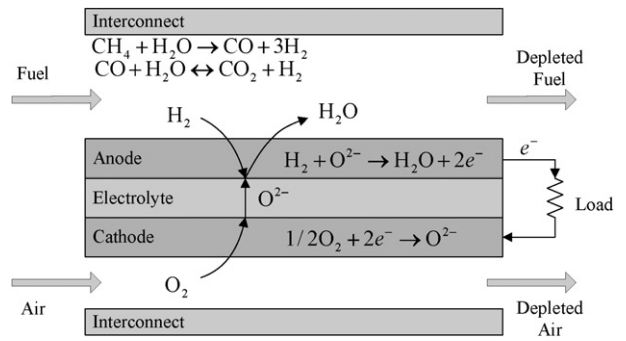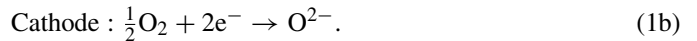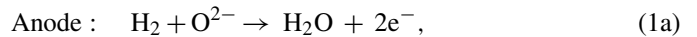

Fig. 1. Schematic diagram of SOFC process.

Table 1
Definitions of fuel utilization and air ratio

Fuel utilization	$U_f = \dfrac{JA/2F}{(4x^{in}_{CH_4} + x^{in}_{H_2} + x^{in}_{CO})N^{in}_{fuel}}$
Air ratio	$AR = \dfrac{x^{in}_{O_2} N^{in}_{air}}{JA/4F}$

can be described as:

$$\text{Anode}: \quad H_2 + O^{2-} \rightarrow H_2O + 2e^-, \tag{1a}$$

$$\text{Cathode}: \tfrac{1}{2}O_2 + 2e^- \rightarrow O^{2-}. \tag{1b}$$

For a direct internal reforming SOFC (DIR-SOFC) that operates on methane, the internal reforming process also takes place in the anode channel to produce hydrogen, and is usually represented by the following steam reforming reaction and water–gas shift (WGS) reaction:

$$\text{Steam reforming}: \quad CH_4 + H_2O \rightarrow CO + 3H_2, \tag{2}$$

$$\text{WGS}: \quad CO + H_2O \leftrightarrow CO_2 + H_2. \tag{3}$$
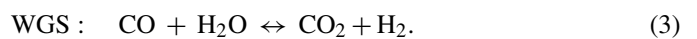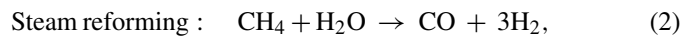
The cell voltage is related to the concentration of electrochemical species by the well-known Nernst equation. In order to provide a voltage greater than zero, not all the reactants in the cell can be consumed [21]. Thus, fuel and air in excess of the required amount of electrochemical reactions should be delivered. In addition, since the electrochemical combination of hydrogen and oxygen is a highly exothermic reaction, excess air is also needed for cell cooling. Two performance factors, i.e. fuel utilization and air ratio (see Table 1) are usually used to define the amount of utilized fuel and excess air, respectively.

3. Development of the dynamic temperature model of SOFC using LS-SVMs

In this section, the LS-SVM regression method is first described. Then issues concerning the development of the dynamic temperature model are discussed in detail, including variable selection, training set construction and hyperparameter tuning.

3.1. LS-SVM for regression

The nonlinear modeling problem based on measurable data essentially is a nonlinear regression problem. The LS-SVM regression model [14,22] employs the following linear representation in a so-called higher dimensional feature space $H \subseteq R^{n_h}$:

$$y(\boldsymbol{x}) = \boldsymbol{w}^{\mathrm{T}} \boldsymbol{\varphi}(\boldsymbol{x}) + b, \tag{4}$$

where $\boldsymbol{x} \in R^n$ is an input vector, $y \in R$ is an output value, $\boldsymbol{w} \in H$ is a feature vector. $\boldsymbol{\varphi}(\cdot) : R^n \rightarrow R^{n_h}$ is a nonlinear mapping from the input space to the feature space, by which a nonlinear regression in the input space is converted to a linear regression in the feature space.

Given a training set $\{\boldsymbol{x}_k, y_k\}_{k=1}^N$, the LS-SVM method considers the regression problem as the following optimization problem:

$$\min_{\boldsymbol{w},b,e} J(\boldsymbol{w}, e) = \frac{1}{2} \boldsymbol{w}^{\mathrm{T}} \boldsymbol{w} + \frac{\gamma}{2} \sum_{k=1}^N e_k^2 \tag{5}$$

subject to equality constraints

$$y_k = \boldsymbol{w}^{\mathrm{T}} \boldsymbol{\varphi}(\boldsymbol{x}_k) + b + e_k, \quad k = 1, \ldots, N, \tag{6}$$

where γ is the regularization parameter, e_k is the prediction error for data point k.

By applying the Lagrangian multiplier method, the solution to above optimization problem is obtained as the following linear equations:

$$\begin{bmatrix} 0 & \mathbf{1}^{\mathrm{T}} \\ \mathbf{1} & \boldsymbol{\Omega} + \gamma^{-1} \mathbf{I} \end{bmatrix} \begin{bmatrix} b \\ \boldsymbol{\alpha} \end{bmatrix} = \begin{bmatrix} 0 \\ \boldsymbol{y} \end{bmatrix} \tag{7}$$

where $\boldsymbol{\alpha} = [\alpha_1, \ldots, \alpha_N]^{\mathrm{T}}$ is the Lagrange multiplier vector, $\boldsymbol{y} = [y_1, \ldots, y_N]^{\mathrm{T}}$, $\mathbf{1} = [1, \ldots, 1]^{\mathrm{T}} \in R^N$, and $\boldsymbol{\Omega}$ is an $N \times N$ kernel matrix. By using the kernel trick [22], one obtains $\Omega_{kl} = \boldsymbol{\varphi}(\boldsymbol{x}_k)^{\mathrm{T}} \boldsymbol{\varphi}(\boldsymbol{x}_l) = K(\boldsymbol{x}_k, \boldsymbol{x}_l)$, $k, l = 1, \ldots, N$. And the resulting LS-SVM regression model becomes

$$y(\boldsymbol{x}) = \sum_{k=1}^N \alpha_k K(\boldsymbol{x}, \boldsymbol{x}_k) + b, \tag{8}$$

where α_k, b are the solution to Eq. (7).

Note that the dot product $\boldsymbol{\varphi}(\cdot)^{\mathrm{T}} \boldsymbol{\varphi}(\cdot)$ in the feature space is replaced by a prechosen kernel function $K(\cdot, \cdot)$ due to the employment of the kernel trick. Thus, there is no need to construct the feature vector $\boldsymbol{w}$ or to know the nonlinear mapping $\boldsymbol{\varphi}(\cdot)$ explicitly. Given a training set, the training of an LS-SVM is equal to solving a set of linear equations as Eq. (7). This greatly simplifies the regression problem.

The chosen kernel function must satisfy the Mercer's condition. The linear, polynomial and radial basis functions kernel are the commonly used kernel functions. In this paper, the popular RBF kernel is used and this is of the form

$$K(\boldsymbol{x}, \boldsymbol{x}_k) = \exp\left(-\frac{||\boldsymbol{x} - \boldsymbol{x}_k||^2}{\sigma^2}\right). \tag{9}$$

3.2. Variable selection of the dynamic temperature model

In order that the resulting dynamic temperature model can be integrated into the whole control scheme of an SOFC, its variables should be selected first according to the employed control scheme.

The aim of controlling an SOFC is to deliver specified electric power to the load and avoid any operating conditions that may cause degradation or damage to the fuel cell. Due to the limitations of components' mechanical properties and the intrinsic nature of establishing the cell voltage mentioned above, the average cell temperature and the supply of fuel and air are the two most important aspects that should be controlled. As the average cell temperature cannot be measured conveniently, in practice a measurable variable, i.e. the outlet fuel temperature is controlled instead [2,3]. The supply of fuel and air can be reflected by the fuel utilization and air ratio, respectively. Hence the common control objectives of an SOFC include: maintaining the fuel utilization as constant as possible; ensuring the air ratio in a certain range; guaranteeing the outlet fuel temperature as constant as possible [2].

These control objectives can be achieved using the control scheme illustrated in Fig. 2. Since the average current density is decided by uncontrollable load, it is taken as a disturbance variable in the control scheme. Fuel and air flow rates are two basic operating degrees of freedom. By measuring the average current density as a feedforward signal, the fuel flow rate calculated according to the definition of fuel utilization can keep the fuel utilization constant. Further, the outlet fuel temperature can be controlled by varying the air ratio, i.e. the supply of air for cooling. F1 and F2 in Fig. 2 are static mappings, which can be obtained from the definitions of fuel utilization and air ratio,
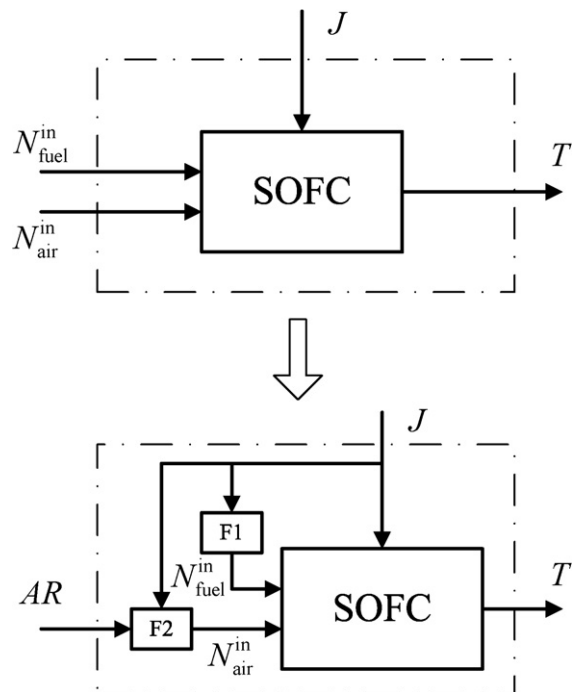

Fig. 2. Control scheme of SOFC.

respectively,

$$N_{\text{fuel}}^{\text{in}} = \text{F1}(J) = \frac{A/2F}{(4x_{\text{CH}_4}^{\text{in}} + x_{\text{H}_2}^{\text{in}} + x_{\text{CO}}^{\text{in}})U_{\text{f}}}J, \qquad (10)$$

$$N_{\text{air}}^{\text{in}} = \text{F2}(J, \text{AR}) = \frac{A/4F}{x_{\text{O}_2}^{\text{in}}}J \cdot \text{AR}, \qquad (11)$$

where U_{f} is the operating fuel utilization. To meet the remaining control objective, what's needed is just to keep the air ratio in a certain range. Therefore, the air ratio is taken as a manipulated variable and the outlet fuel temperature as a controlled variable in the control scheme. Correspondingly in our dynamic temperature model, the average current density and the air ratio are two input variables, and the outlet fuel temperature is an output variable. The inlet gas temperature and composition herein are assumed to be fixed.

As the NARX model is a general model structure suitable for representing a wide class of nonlinear dynamic systems, it is used to describe the nonlinear temperature dynamics of an SOFC in this study. The dynamic temperature model thereby can be written as:

$$T_k = f(T_{k-1}, \ldots, T_{k-n_y}, J_{k-1}, \ldots, J_{k-n_d}, \text{AR}_{k-1}, \ldots,$$
$$\text{AR}_{k-n_u}), \qquad (12)$$

where T_k, J_k, and AR_k represent the outlet fuel temperature, the average current density and the air ratio at sampling instant k, respectively, n_y, n_d and n_u are the maximum lags of T, J and AR, respectively, which are determined by the specific process data, $f(\cdot)$ is an unknown nonlinear mapping. Let $y_k = T_k$ and $\boldsymbol{x}_k = [T_{k-1}, \ldots, T_{k-n_y}, J_{k-1}, \ldots, J_{k-n_d}, \text{AR}_{k-1}, \ldots, \text{AR}_{k-n_u}]^{\text{T}}$. Thus, the dynamic temperature modeling problem could be stated as: build an LS-SVM regression model in the form of Eq. (8) based on a training set $\{\boldsymbol{x}_k, y_k\}_{k=1}^N$ to approximate the nonlinear mapping $f(\cdot)$.

3.3. Construction of training data set

Constructing a training set containing sufficient representative data points is an important step in building an LS-SVM model that can represent SOFC's temperature dynamics over a relatively wide operating range. The basic guideline on constructing a training set is that the data in it should cover the entire expected operating range of the LS-SVM model. As analyzed in Section 3.2, the dynamic temperature model has two input variables J, AR and one output variable T. Hence the expected operating ranges of all the three variables should be covered.

In this study, the training data is generated with a physical SOFC model (see Appendix A). A scheme consisting of a set of operating cases is designed to collect training data by the physical model (refer to Section 4.1). Each operating case is determined by three parameters: J, AR and the initial temperature T_0. Several levels of J and AR, which distribute uniformly over their respective operating ranges, are selected, and each level of J and AR should be included in the scheme. Moreover, the T_0 of each case should ensure that its corresponding temperature dynamic process can cover the expected operating range

of T as widely as possible. Thus, the lower or upper bound of the expected operating range of T is usually selected as T_0. After resampled, the dynamic data of these operating cases can be used to construct the training set. To reduce the amount of training data, at first only the data of part of these cases are added to the training set. Then, the data of other cases are added gradually until satisfactory modeling results are achieved. This approach guarantees that the training set can contain enough representative data points in a relatively small size.

3.4. Tuning hyperparameters automatically by GA

With the RBF kernel chosen a priori, there are two parameters that need to be tuned, i.e. the regularization parameter γ in Eq. (5) and the kernel parameter σ^2 in Eq. (9). The two parameters are usually referred to as hyperparameters. Choosing an optimal set of hyperparameters is also an important step in LS-SVM design. The aim of tuning the hyperparameters is to make the LS-SVM model achieve better generalization ability (i.e. the ability to correctly predict samples that are not contained in the training set), which is usually evaluated using an estimated generalization error [23]. Consequently, the problem of hyperparameter tuning is equal to looking for a set of hyperparameters in the search space that can minimize the estimated generalization error. In this paper, the genetic algorithm is employed to implement the task of optima searching. The simplicity and high efficiency of GA can help to accurately find the optimal hyperparameters in a relatively low time cost.

GA is a form of evolutionary algorithm, which is invented by John Holland and has achieved notable success on various hard optimization problems [19,20]. The basic idea of GA originates from the mechanisms of evolution and the principle of natural selection in nature. GA starts with an initial set of random solutions called population. Each individual in the population represents a feasible solution to the problem at hand. The population "evolves" through successive iterations, called generations. At each generation, the individuals are evaluated using some measures of fitness, and a series of genetic operations including selection, crossover and mutation are imposed upon individuals in the current population to create the next generation. After several generations, the algorithm may converge to the best individual, which hopefully represents the optimal solution to the problem. During the implementation of GA, what's needed is just the information of fitness. This is a prominent difference between GA and classical, derivative-based, optimization algorithms.

For the problem of hyperparameter tuning by GA, each set of γ and σ^2 is taken as an individual in a population, and the estimated generalization error as the fitness. As the k-fold cross-validation is a very reliable method to estimate the generalization error [23], it is employed in this paper. In k-fold cross-validation, the training data is randomly split into k roughly equal subsets. An LS-SVM decision rule is trained using $(k-1)$ of these subsets and validated on the subset left out. This procedure is repeated k times with each of the k subsets used as the validation subset in turn. Averaging the validation errors over the k trials gives an estimate of the generalization error. The flow-
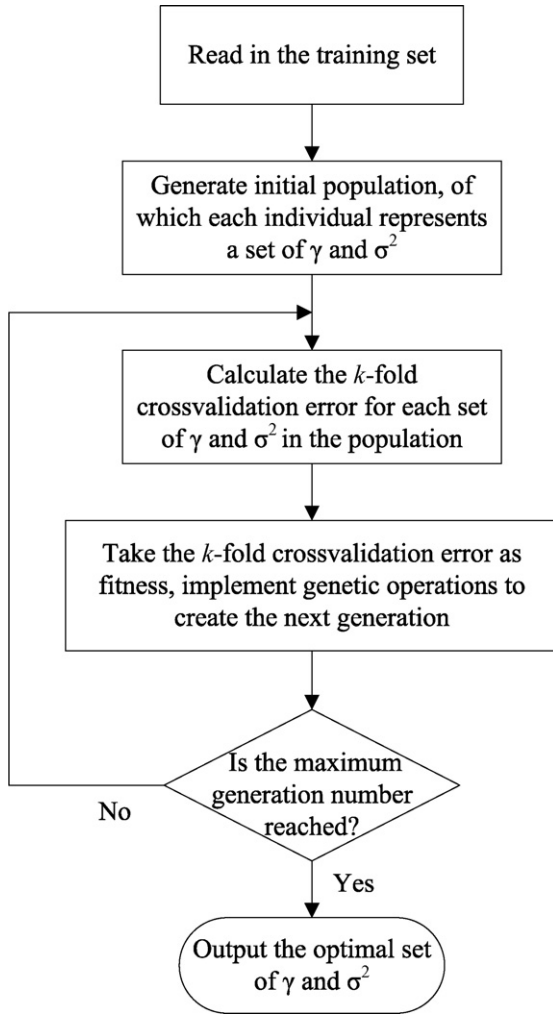
Fig. 3. Flowsheet of hyperparameter tuning.

sheet of tuning the hyperparameters by GA is illustrated in Fig. 3.

4. Modeling results and model validation

4.1. Modeling results

A planar SOFC in a co-flow configuration is adopted in our modeling. This is a single square electrolyte-supported SOFC operating with direct internal steam reforming of methane and air. The parameters and design operating conditions of the SOFC are listed in Table 2. The expected operating ranges of the LS-SVM temperature model are $J \in [2000, 3500]$ A m^{-2}, AR $\in [5, 8]$ and $T \in [1247, 1347]$ K, which include the design point of the SOFC. To collect training data, four levels of J and AR are selected, respectively, and a scheme containing 16 operating cases is designed (see Table 3, the cases that are not used have been omitted). By solving the physical model using the fourth-order Runge–Kutta method [27], the input and output data of the 16 cases are collected and then resampled using a sampling interval of 220 s. The maximum lags n_y, n_d and n_u in Eq. (12)

are determined by a trial method, and herein $[n_y, n_d, n_u]^{\mathrm{T}} = [1, 1, 1]^{\mathrm{T}}$ is employed. Finally the training set $\{x_k, y_k\}_{k=1}^{960} \subset R^3 \times R$ is obtained.

The two-dimensional search space of γ and σ^2 is $[1, 10^4] \times [0.1, 10^3]$. The population size and the maximum generation number are set to 15 and 25, respectively. By the proposed GA-based tuning method with the 5-fold cross-validation error as fitness, it takes 7.42 h to find the optimal set of (γ, σ^2) at (8709, 33.01) on an AMD Sempron$^{\mathrm{TM}}$ 1.6 GHz computer with 512 MB RAM. The best and mean fitness values in each generation are illustrated in Fig. 4. Then an LS-SVM model is obtained using the optimal hyperparameter values.

Table 2
Parameters and assumed operating conditions of the SOFC

Cell parameters [24–26]	
Cell number	1
Cell active area (m^2)	0.1×0.1
Anode thickness (m)	5×10^{-5}
Cathode thickness (m)	5×10^{-5}
Electrolyte thickness (m)	1.5×10^{-4}
Anode volume (m^3)	5.4×10^{-6}
Cathode volume (m^3)	5.4×10^{-6}
Mass (kg)	0.2668
Density (kg m^{-3})	6600
Heat capacity (J kg^{-1} K^{-1})	400
Anode electrical conductivity (Ω^{-1} m^{-1})	$(9.5 \times 10^7/T) \exp(-1150/T)$
Cathode electrical conductivity (Ω^{-1} m^{-1})	$(4.2 \times 10^7/T) \exp(-1200/T)$
Electrolyte electrical conductivity (Ω^{-1} m^{-1})	$3.34 \times 10^4 \exp(-10,300/T)$
Limiting current density (A m^{-2})	8000
Activation energy of anode (J mol^{-1})	1×10^5
Activation energy of cathode (J mol^{-1})	1.17×10^5
Pre-exponential factor of anode (A m^{-2})	5.5×10^8
Pre-exponential factor of cathode (A m^{-2})	7.0×10^8
Assumed operating conditions	
Average current density (A m^{-2})	3000
Fuel utilization	0.85
Air ratio	7
Operating pressure (bar)	1
Inlet gas temperature (K)	1123
Inlet gas composition	Fuel: H_2, 0.2626; CH_4, 0.171; H_2O, 0.4924; CO, 0.0194; CO_2, 0.0436 Air: O_2, 0.21; N_2, 0.79

Table 3
Operating cases for constructing the training set

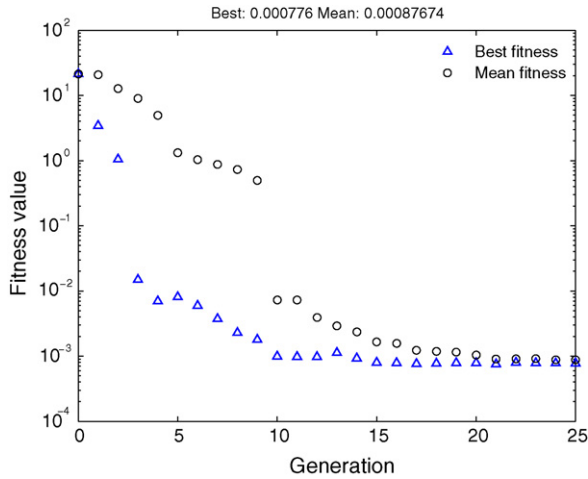| Case	J (A m^{-2})	AR	T_0 (K)	Case	J (A m^{-2})	AR	T_0 (K)
1	2000	5	1247	9	3000	5	1247
2	2000	6	1247	10	3000	6	1247
3	2000	7	1247	11	3000	7	1247
4	2000	8	1247	12	3000	8	1247
5	2500	5	1247	13	3500	5	1247
6	2500	6	1247	14	3500	6	1247
7	2500	7	1247	15	3500	7	1247
8	2500	8	1247	16	3500	8	1247

Fig. 4. Best and mean fitness values in each generation.

4.2. Model validation

First it is necessary to note that there are two different modes of operation of a trained LS-SVM NARX model: the series–parallel mode and the parallel mode [28]. Eq. (12) represents the series–parallel mode. The LS-SVM model operating in this mode requires both input and output data from the process as inputs and can predict the process output only one time step into the future. On the other hand, the LS-SVM model operating in the parallel mode has the following form:

$$\hat{T}_k = f(\hat{T}_{k-1}, \ldots, \hat{T}_{k-n_y}, J_{k-1}, \ldots, J_{k-n_d}, AR_{k-1}, \ldots,$$
$$AR_{k-n_u}), \tag{13}$$

where the output of the LS-SVM model $\hat{T}_k$ is delayed and fed back to the model inputs to predict the process output further into the future. In this parallel mode, the LS-SVM model can be used independently from the process and provide long range predictions from only process input information. Obviously an LS-SVM model that can operate accurately in the parallel mode

is a more powerful tool for designing control strategies than that can operate accurately only in the series–parallel mode. However, the parallel mode has higher requirements for the prediction accuracy of the LS-SVM model, because the prediction error in one step may accumulate to a bigger one after multiple steps. To fully verify its ability to represent the temperature dynamics of the SOFC, in this section the LS-SVM model is operated in both the two modes and the associated mean squared errors (MSEs) in both modes are calculated.

Two sets of validation tests (see Table 4), which are, respectively, called Validation A and Validation B in this paper, are carried out to validate the LS-SVM model. Validation A is to compare the temperature dynamics of the LS-SVM model with that of the physical model under operating cases that are not used during training. The twelve validation cases in Validation A cover the main operating region of the LS-SVM model. In Validation B, the LS-SVM model is tested on two different step inputs (AR and J) and the corresponding responses are compared with those of the physical model.

The MSEs of each validation case are listed in Table 4. It is found that the LS-SVM model operating in the series–parallel mode can reproduce the temperature dynamics of the SOFC with high accuracy for each validation case. As expected, the MSE in the parallel mode is bigger than that in the series–parallel mode for each case. The biggest MSE is 1.7255 for Case A12, which indicates that the maximum root mean squared error (RMSE) of the temperature prediction is less than 1.5 K. This is still very satisfactory for multi-step ahead prediction. Figs. 5–7 illustrate the temperature responses of the LS-SVM model operating in the parallel mode along with the comparison with those of the physical model. The corresponding figures of the series–parallel mode are omitted here due to similarity and their higher accuracy. It can be seen from these figures that the temperature responses of the LS-SVM model show good consistency with those of the physical model. All these validation results demonstrate that the LS-SVM model is capable of emulating the temperature dynamics of the SOFC with good accuracy from only process input data.

Table 4
Validation cases and associated MSEs

|	Case	J (A m^{-2})	AR	T_0 (K)	MSE in series–parallel mode (K^2)	MSE in parallel mode (K^2)
	A1	3300	6.5	1247	0.0067	0.3034
	A2	2800	6.5	1247	0.0009	0.0327
	A3	2300	6.6	1247	0.0069	0.4979
	A4	3300	6.5	1347	0.0097	0.5304
	A5	2800	6.5	1347	0.0015	0.1028
Validation A	A6	2300	6.5	1347	0.0060	0.5439
	A7	3300	7.5	1247	0.0004	0.0085
	A8	2800	7.5	1247	0.0042	0.1877
	A9	2300	7.5	1247	0.0067	0.3062
	A10	3300	7.5	1347	0.0006	0.0044
	A11	2800	7.5	1347	0.0061	0.2614
	A12	2300	7.5	1347	0.0294	1.7255
	Case	Input signal description			MSE in series–parallel mode (K^2)	MSE in parallel mode (K^2)
Validation B	B1	Step input of AR with fixed $J = 3000$ A m^{-2}			0.0084	0.8152
	B2	Step input of J with fixed AR $= 7$			0.0093	0.8024
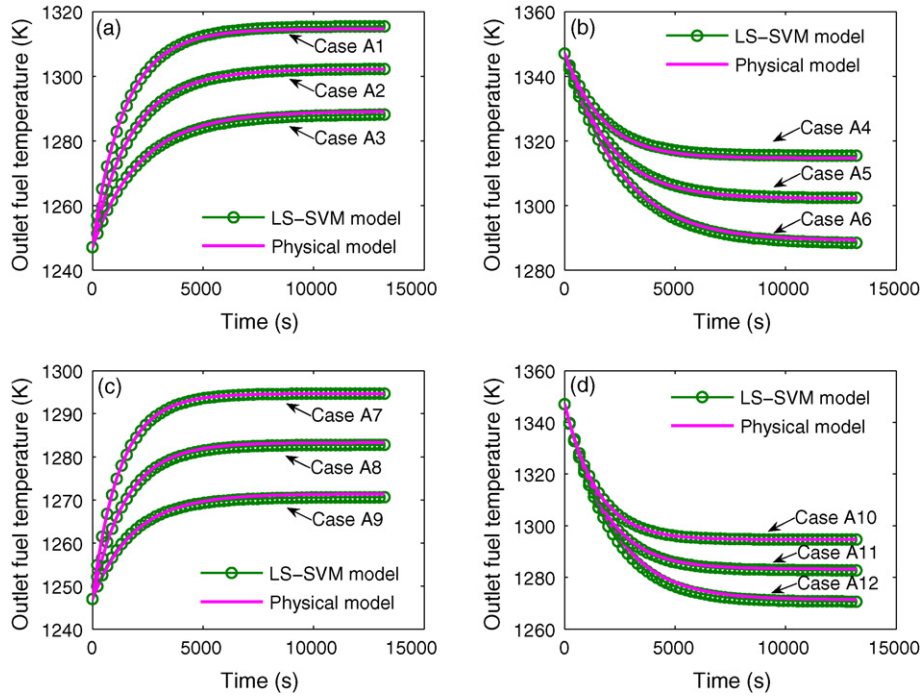
Fig. 5. Temperature responses of the LS-SVM model operating in a parallel mode and the physical model for Validation A: (a) Cases A1–A3; (b) Cases A4–A6; (c) Cases A7–A9; (d) Cases A10–A12.
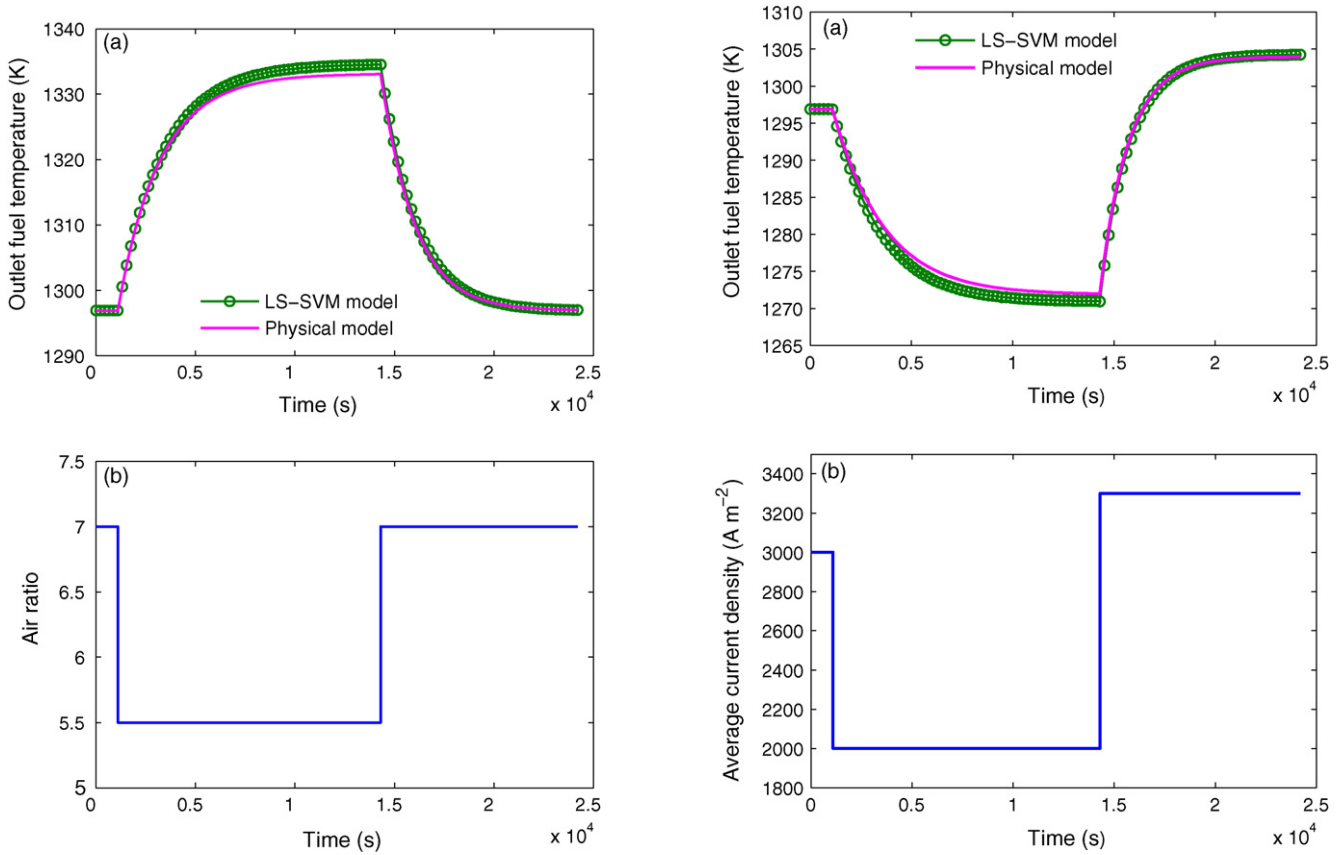

Fig. 6. Temperature responses of the LS-SVM model operating in a parallel mode and the physical model for Case B1: (a) temperature responses; (b) step signal of AR.

Fig. 7. Temperature responses of the LS-SVM model operating in a parallel mode and the physical model for Case B2: (a) temperature responses; (b) step signal of J.

5. Conclusions

A dynamic temperature model of an SOFC is developed in this paper using least squares support vector machines (LS-SVMs). Issues concerning the development of the LS-SVM temperature model, including variable selection, training set construction and hyperparameter tuning, are discussed. Comprehensive validation tests have shown that the developed LS-SVM model is sufficiently accurate to emulate the temperature response of the SOFC over a relatively wide operating range using only process input information. The powerful ability of the LS-SVM temperature model benefits from the approaches of constructing the training set and tuning the hyperparameters automatically by GA, besides the modeling method itself. In this study, the training data is generated with a physical model. If sufficient data from a real plant is obtained, the optimal LS-SVM temperature model of SOFC can be built automatically in the same way.

The LS-SVM temperature model presented in this paper is useful for designing temperature control strategies. Control of the SOFC using the LS-SVM model will be the focus of our future work.

Acknowledgement

Appendix A. A physical model of DIR-SOFC

This model is developed based on conservation laws and electrochemical principles. Several assumptions are made as follows:

(1) Three reactions (1)–(3) are included in the model.
(2) The temperature of the solid part (including the PEN and interconnect) and the molar fraction of each gas species distribute uniformly over the SOFC, i.e. the SOFC is treated as a well-stirred reactor [29,30].
(3) The outlet stream temperature is equal to the solid temperature: $T^{\text{out}} = T^{\text{s}}$ [29,30]. For simplicity, they are also denoted by T in this paper.
(4) The rate of energy accumulation in the gas phase is negligible with respect to the solid part [29–31].

A.1. Mass balance equations

The molar balance is applied to each gas species within the SOFC as follows:

$$\text{Anode}: \quad \frac{k_p p_{\text{an}} V_{\text{an}}}{RT} \frac{dx_i}{dt} = N_{\text{an}}^{\text{in}} x_i^{\text{in}} - N_{\text{an}}^{\text{out}} x_i^{\text{out}} + \sum_{j=1}^{\xi} a_{ij} r_j,$$

$$i \in \{CH_4, H_2, CO, CO_2, H_2O\}, \tag{A.1}$$

$$\text{Cathode}: \quad \frac{k_p p_{\text{ca}} V_{\text{ca}}}{RT} \frac{dx_i}{dt} = N_{\text{ca}}^{\text{in}} x_i^{\text{in}} - N_{\text{ca}}^{\text{out}} x_i^{\text{out}} + \sum_{j=1}^{\xi} a_{ij} r_j,$$

$$i \in \{O_2, N_2\}, \tag{A.2}$$

where $k_p = 10^5 \, \text{Pa bar}^{-1}$, x_i is the molar fraction of species i, a_{ij} the stoichiometric coefficient of species i in reaction j, and r_j the rate of reaction j.

The reaction rates of (1)–(3) are calculated by the following equations [25]:

$$r_1 = \frac{AJ}{n_e F}, \tag{A.3}$$

$$r_2 = A_r k_r p_{\text{an}} x_{CH_4} \exp\left(\frac{-E_{\text{a,r}}}{RT}\right), \tag{A.4}$$

$$r_3 = A_{\text{sh}} k_{\text{sh}} p_{\text{an}}(x_{CO} x_{H_2O} - K_{\text{sh}} x_{CO_2} x_{H_2}), \tag{A.5}$$

where the activation energy of reforming reaction $E_{\text{a,r}} = 82000 \, \text{J mol}^{-1}$, the equilibrium constant of WGS reaction K_{sh} is obtained using the method of Ref. [32].

According to the continuity equations, the outlet total molar flow rate is calculated by

$$N_{\text{an}}^{\text{out}} = N_{\text{an}}^{\text{in}} + 2r_2, \qquad N_{\text{ca}}^{\text{out}} = N_{\text{ca}}^{\text{out}} - \frac{r_1}{2}. \tag{A.6}$$

A.2. Energy balance equation

The energy conservation law is used for the whole SOFC and the energy balance equation [25,31] is written as

$$M^{\text{s}} C_p^{\text{s}} \frac{dT^{\text{s}}}{dt} + \sum_{k=1}^{2} \sum_{i=1}^{\zeta_k} \frac{dn_i h_i}{dt}$$

$$= \sum_{k=1}^{2} \sum_{i=1}^{\zeta_k} \left(N_i^{\text{in}} \int_{T^{\text{ref}}}^{T^{\text{in}}} c_{pi} \, dT - N_i^{\text{out}} \int_{T^{\text{ref}}}^{T^{\text{out}}} c_{pi} \, dT \right) - Q_{\text{gen}}, \tag{A.7}$$

where $\zeta_1 = 5$ for CH_4, H_2, CO, CO_2, H_2O, $\zeta_2 = 2$ for O_2, N_2.

The first term on the left side of Eq. (A.7) is the rate of energy accumulation in the solid part of the SOFC and the second term, which can be neglected because of the fourth assumption, is that in the gases. The first term on the right side is the enthalpy change due to the input and output gas streams, the second term is the heat generated by the three reactions and is calculated by

$$Q_{\text{gen}} = \Delta H_1 r_1 + \Delta H_2 r_2 + \Delta H_3 r_3 - P_{\text{dc}}. \tag{A.8}$$

The gas specific heat c_{pi} in Eq. (A.7) is a function of temperature:

$$c_{pi}(T) = b_0 + b_1 T + b_2 T^2 + b_3 T^3. \tag{A.9}$$

A.3. Voltage model

The output voltage is calculated by subtracting three kinds of overpotential losses, i.e. ohmic, activation and concentration overpotentials, from the reversible voltage as Eq. (A.10).

$$U = U_N - \eta_{\text{ohm}} - \eta_{\text{act}} - \eta_{\text{conc}} \tag{A.10}$$

The reversible voltage U_N is calculated by the Nernst equation:

$$U_N = U_0(T) + \frac{RT}{2F} \ln \left[\frac{x_{H_2} x_{O_2}^{0.5} p_{ca}^{0.5}}{x_{H_2O}} \right], \tag{A.11}$$

with $U_0(T) = 1.2723 - 2.7645 \times 10^{-4} T$, where $U_0(T)$ is the reversible voltage at standard pressure [33].

The ohmic overpotential is calculated by the Ohm's law as:

$$\eta_{ohm} = J R_{ohm}, \tag{A.12}$$

where R_{ohm} is the internal resistance of the cell and is calculated from the conductivity of the individual layers [6] by

$$R_{ohm} = \frac{\tau_{an}}{\sigma_{an}} + \frac{\tau_{elec}}{\sigma_{elec}} + \frac{\tau_{ca}}{\sigma_{ca}}. \tag{A.13}$$

The activation overpotential is given by:

$$\eta_{act} = \frac{2RT}{n_e F} \sinh^{-1} \left(\frac{J}{2 j_{0,an}} \right) + \frac{2RT}{n_e F} \sinh^{-1} \left(\frac{J}{2 j_{0,ca}} \right), \tag{A.14}$$

where $j_{0,an}$ and $j_{0,ca}$ denote the anodic and cathodic exchange current density, respectively, and are modeled in the following form [34]:

$$j_{0,an} = \beta_{an} \left(\frac{p_{an} x_{H_2}}{p^{ref}} \right) \left(\frac{p_{an} x_{H_2O}}{p^{ref}} \right) \exp \left(-\frac{E_{a,an}}{RT} \right), \tag{A.15}$$

$$j_{0,ca} = \beta_{ca} \left(\frac{p_{ca} x_{O_2}}{p^{ref}} \right)^{0.25} \exp \left(-\frac{E_{a,ca}}{RT} \right). \tag{A.16}$$

The concentration overpotential is determined from

$$\eta_{conc} = -\frac{RT}{2F} \ln \left(1 - \frac{J}{j_L} \right), \tag{A.17}$$

where j_L is the limiting current density.

References

[1] S.C. Singhal, K. Kendall (Eds.), High Temperature Solid Oxide Fuel Cells: Fundamentals, Design and Applications, Elsevier Advanced Technology, UK, 2003, pp. 14–19.

[2] P. Aguiar, C.S. Adjiman, N.P. Brandon, J. Power Sources 147 (2005) 136–147.

[3] C. Stiller, B. Thorud, O. Bolland, R. Kandepu, L. Imsland, J. Power Sources 158 (2006) 303–315.

[4] E. Achenbach, J. Power Sources 49 (1994) 333–348.

[5] D.J. Hall, R.G. Colclaser, IEEE Trans. Energy Conv. 14 (1999) 749–753.

[6] P. Aguiar, C.S. Adjiman, N.P. Brandon, J. Power Sources 138 (2004) 120–136.

[7] H. Xi, J. Sun, V. Tsourapas, J. Power Sources 165 (2007) 253–266.

[8] D.E. Seborg, T.F. Edgar, D.A. Mellichamp, Process Dynamics and Control, second ed., John Wiley & Sons, 2004, pp. 157–181.

[9] L. Ljung, System Identification—Theory for the User, second ed., Prentice Hall, New York, 1999.

[10] C. Shen, G.-Y. Cao, X.-J. Zhu, Simulat. Model. Pract. Theor. 10 (2002) 109–119.

[11] F. Jurado, J. Power Sources 154 (2006) 145–152.

[12] F. Jurado, J. Power Sources 158 (2006) 245–253.

[13] F. Yang, X.-J. Zhu, G.-Y. Cao, J. Power Sources 166 (2007) 354–361.

[14] J.A.K. Suykens, J. Vandewalle, Neural Process. Lett. 9 (1999) 293–300.

[15] J.A.K. Suykens, J. Vandewalle, B. De Moor, Neural Netw. 14 (2001) 23–35.

[16] S. Viaene, B. Baesens, T. Van Gestel, J.A.K. Suykens, D. Van den Poel, D. Dedene, B. De Moor, J. Vanthienen, Int. J. Intell. Syst. 16 (2001) 1023–1036.

[17] C.-M. Vong, P.-K. Wong, Y.-P. Li, Eng. Appl. Artif. Intell. 19 (2006) 277–287.

[18] H.-B. Huo, X.-J. Zhu, G.-Y. Cao, J. Power Sources 162 (2006) 1220–1225.

[19] J.H. Holland, Adaptation in Natural and Artificial Systems, University of Michigan Press, Ann Arbor, 1975.

[20] D.E. Goldberg, Genetic Algorithm in Search, Optimization, and Machine Learning, Addison-Wesley, Reading, MA, 1989.

[21] J. Larminie, A. Dicks, Fuel Cell Systems Explained, John Wiley & Sons, 2000, p. 32.

[22] J.A.K. Suykens, Eur. J. Contr. (Special Issue on fundamental issues in control) 7 (2001) 311–327.

[23] K. Duan, S.S. Keerthi, A.N. Poo, Neurocomputing 51 (2003) 41–59.

[24] J.R. Ferguson, J.M. Fiard, R. Herbin, J. Power Sources 58 (1996) 109–122.

[25] X. Zhang, J. Li, G. Li, Z. Feng, J. Power Sources 160 (2006) 258–267.

[26] A. Selimovic, Doctoral Thesis, Lund University, Sweden, 2002.

[27] J.H. Mathews, K.D. Fink, Numerical Methods Using Matlab, fourth ed., Prentice Hall, 2003.

[28] K.S. Narendra, K. Parthasarathy, IEEE Trans. Neural Netw. 1 (1990) 4–27.

[29] M.D. Lukas, K.Y. Lee, H. Ghezel-Ayagh, IEEE Trans. Energy Conv. 14 (1999) 1651–1657.

[30] R. Kandepu, L. Imsland, B.A. Foss, C. Stiller, B. Thorud, O. Bolland, Energy 32 (2007) 406–417.

[31] A.M. Murshed, B. Huang, K. Nandakumar, J. Power Sources 163 (2007) 830–845.

[32] H. Yakabe, T. Ogiwara, M. Hishinuma, I. Yasuda, J. Power Sources 102 (2001) 144.

[33] S. Campanari, P. Iora, J. Power Sources 132 (2004) 113–126.

[34] P. Costamagna, K. Honegger, J. Electrochem. Soc. 145 (1998) 3995–4007.